6706 *Inorg. Chem.* **2010**, *49*, 6706–6715
DOI: 10.1021/ic100953m

Inorganic Chemistry
Article

Ln^{3+} (Ln = Eu, Dy, Sm, and Er) Ion-Doped YVO_4 Nano/Microcrystals with Multiform Morphologies: Hydrothermal Synthesis, Growing Mechanism, and Luminescent Properties

Zhenhe Xu, Xiaojiao Kang, Chunxia Li,* Zhiyao Hou, Cuimiao Zhang, Dongmei Yang, Guogang Li, and Jun Lin*

State Key Laboratory of Rare Earth Resource Utilization, Changchun Institute of Applied Chemistry, Chinese Academy of Sciences, Changchun 130022, and Graduate University of the Chinese Academy of Sciences, Beijing 100049, P.R. China

Received May 13, 2010

YVO_4 nano/microcrystals with multiform morphologies, such as nanoparticles, microdoughnut, micropancake, pillar structure, and microflower, have been synthesized via a facile hydrothermal route. A series of controlled experiments indicate that the shape and size of as-prepared architectures can be tuned effectively by controlling the reaction conditions, such as reaction time, vanadium sources, different organic additives, and the molar ratio of organic additive trisodium citrate (Cit^{3-}):Y^{3+}. It is found that Cit^{3-} as a ligand and shape modifier has the dynamic effect by adjusting the growth rate of different facets under different experimental conditions, resulting in the formation of various geometries of the final products. The possible formation mechanisms for products with diverse architectures have been presented in detail. Additionally, we systematically investigate the luminescent properties of the YVO_4:Ln^{3+} (Ln = Eu, Dy, Sm, and Er). Because of an efficient energy transfer from vanadate groups to dopants, YVO_4:Ln^{3+} (Ln = Eu, Dy, Sm, and Er) phosphors showed their strong characteristic emission under ultraviolet excitation and low-voltage electron beam excitation. The ability to generate YVO_4 nano/microstructures with diverse shapes, multicolor emission, and higher quantum efficiency provides a great opportunity for systematically evaluating their luminescence properties, as well as fully exploring their applications in many types of color display fields.

1. Introduction

In recent years, the design and synthesis of inorganic nano/microcrystals with well-defined morphologies and accurately tunable sizes remains the research focus and one of the challenging issues, because it is well-known that the properties of the materials closely interrelate with geometrical factors such as shape, dimensionality, and size.[1] Therefore, many efforts have been made to fabricate a range of inorganic crystals in different systems to enhance their performance in currently existing applications.[2] Although some progress has been made in the preparation of highly organized building blocks of metals,[3] semiconductors,[4,5] copolymers,[6] organic–inorganic hybrid materials,[7] and biomaterials[8] based on different driving mechanisms, effective large-scale preparation of some functional nano/micromaterials is still a challenge to material scientists. Nanomaterials have many interesting properties that differ from those of the bulk materials.[9] However, most nanomaterials often have a natural tendency toward aggregation, which is always assumed to be the main hindrance to their practical application. Recently, extensive work has been devoted to the investigation of complex microarchitectures, especially, three-dimensional (3D) hierarchical architectures assembled by nanostructured building blocks such as nanoplates, nanoparticles, nanoribbons, and nanorods.[10] It is

---

*To whom correspondence should be addressed. E-mail: cxli@ciac.jl.cn (C.X.L.), jlin@ciac.jl.cn (J.L.).

(1) (a) Alivisatos, A. P. *Science* **1996**, *271*, 933. (b) Hu, J.; Odom, T. W.; Lieber, C. M. *Acc. Chem. Res.* **1999**, *32*, 435. (c) Wang, X.; Zhuang, J.; Peng, Q.; Li, Y. D. *Nature* **2005**, *437*, 121. (d) Chan, T. S.; Liu, R. S.; Baginskiy, I. *Chem. Mater.* **2008**, *20*, 1215. (e) Wang, Z. L.; Hao, J. H.; Chan, H. L. W. *J. Mater. Chem.* **2010**, *20*, 3178.

(2) (a) Li, C. X.; Hou, Z. Y.; Zhang, C. M.; Yang, P. P.; Li, G. G.; Xu, Z. H.; Fan, Y.; Lin, J. *Chem. Mater.* **2009**, *21*, 4598. (b) Kang, C. C.; Liu, R. S.; Chang, J. C.; Lee, B. J. *Chem. Mater.* **2003**, *15*, 3966. (c) Zhou, S. F.; Jiang, N.; Wu, B.; Hao, J. H.; Qiu, J. R. *Adv. Funct. Mater.* **2009**, *19*, 2081.

(3) Kaltenpoth, G.; Himmelhaus, M.; Slansky, L.; Caruso, F.; Grunze, M. *Adv. Mater.* **2003**, *15*, 1113.

(4) Yada, M.; Taniguchi, C.; Torikai, T.; Watari, T.; Furuta, S.; Katsuki, H. *Adv. Mater.* **2004**, *16*, 1448.

(5) Fan, H. Y.; Yang, K.; Boye, D. M.; Sigmon, T.; Malloy, K. J.; Xu, H.; López, G. P.; Brinker, C. J. *Science* **2004**, *304*, 567.

(6) (a) Jenekhe, S. A.; Chen, X. L. *Science* **1998**, *279*, 1903. (b) Ikkala, O.; Brinke, G. T. *Science* **2002**, *295*, 2407.

(7) Du, J.; Chen, Y. *Angew. Chem., Int. Ed.* **2004**, *43*, 5084.

(8) Shenton, W.; Pum, D.; Sleytr, U. B.; Mann, S. *Nature* **1997**, *389*, 585.

(9) (a) Sun, S.; Weiss, S.; Alivisatos, A. P. *Science* **1998**, *281*, 2013. (b) Luo, W. Q.; Li, R. F.; Liu, G. K.; Antonio, M. R.; Chen, X. Y. *J. Phys. Chem. C* **2008**, *112*, 10370. (c) Fu, C. Y.; Liao, J. S.; Luo, W. Q.; Li, R. F.; Chen, X. Y. *Opt. Lett.* **2008**, *33*, 953.

(10) (a) Yang, J.; Li, C. X.; Zhang, X. M.; Quan, Z. W.; Zhang, C. M.; Li, H. Y.; Lin, J. *Chem.–Eur. J.* **2008**, *14*, 4336. (b) Zhen, L.; Xu, C. Y.; Yang, L.; Shao, W. Z. *Cryst. Growth Des.* **2008**, *8*, 1734.

very useful for practical application that this kind of materials not only possesses some improved properties originating from their building blocks, named nanocrystals, but also solves the problem of nanoparticle agglomeration.[10a] On the other hand, such materials are not only a crucial step for the realization of "bottom-up" techniques for future nanodevices but also offer opportunities to explore their novel collective optical, mechanical, magnetic, and electronic properties.[11] There have been extensive studies to explore approaches to the synthesis of hierarchical materials, such as flower-like $SrCO_3$ superarchitectures,[10b] hierarchical ZnO nanostructures,[12] dandelion-like ZnS microspheres,[13] urchin-like $NaY(MoO_4)_2$.[14] Therefore, it is still a big challenge to develop simple and reliable synthetic methods for hierarchical architectures with designed chemical components and controlled morphologies, which strongly affect the properties of nano/micromaterials.

Recently, much research attention has been paid to the field of rare earth materials since they have many potential applications based on their novel electronic and optical properties resulting from their 4f electrons.[15] Among the various rare earth materials, lanthanide orthovanadates have many wonderful characteristics including excellent thermal, mechanical, and optical properties; especially they play an important role in many optical devices, catalysts, and laser host materials.[16−18] In particular, yttrium vanadate (YVO_4) is an important oxide in materials science and technology, for example, its large single crystal has been extensively used as an excellent polarizer and laser host material, whereas its powder doped with several rare earth ions has been used as an attractive phosphor owing to its high luminescence quantum yield (QY).[19] The previous work mainly focused on the Eu^{3+}-doped YVO_4 with different synthetic methods,[20] because it is a significant commercial red-emitting phosphor used in color television, the high-pressure mercury lamp, and as a scintillator in medical image detectors.[21] Although a lot of efforts had been devoted to the chemical synthesis of YVO_4 nano/microstructures, including hydro-/solvothermal method,[22] sol−gel process,[23] solution combustion synthesis,[24] microemulsion,[25] coprecipitation reaction,[26] and so on. From the perspective of application, nano/micromaterials are not only synthesized in large quantities with desired composition, reproducible size, shape, and structure but also prepared and assembled using green, environmentally responsible methodologies. Compared with the synthesis in the organic solvents, a water-based system should provide a relatively green chemical alternative to the preparation of various nano/micromaterials. Moreover, a water-based system also provides a number of other merits such as simplicity, safety, convenience, and the potential for large-scale production. For these reasons, the water-based systems as a more attractive route to the shape-controlled synthesis of nano/micromaterials have recently received more and more attention.[27]

In this paper, we demonstrate a general strategy for the synthesis of YVO_4 nano/microstructures via a complexing-agent assisted hydrothermal approach. The shape and dimensionality of the obtained YVO_4 architectures can be controlled by adjusting reaction time, vanadium sources, different organic additives, and the molar ratio of organic additive trisodium citrate (Cit^{3-}):Y^{3+}. Then we concentrate on the luminescence properties of YVO_4 doped with different Ln^{3+} (Ln = Eu, Dy, Sm, and Er) ions in an effort to adjust the emission colors and intensity of the final products.

2. Experimental Section

2.1. Preparation. The rare earth oxides RE_2O_3 (RE = Y, Sm, Eu, Dy, and Er) (99.99%), were purchased from Science and Technology Parent Company of Changchun Institute of Applied Chemistry, and other chemicals were purchased from Beijing Chemical Company, China. All chemicals are of analytical grade reagents and were used directly without further purification. Rare earth chloride stock solutions of 0.2 M were prepared by dissolving the corresponding metal oxide in hydrochloric acid at elevated temperature. In a typical procedure, 10 mL of YCl_3 (0.2 M) was added into 20 mL of aqueous solution containing 4 mmol of trisodium citrate (labeled as Cit^{3-}) to form the Y^{3+}-Cit^{3-} complex (2:1 molar ratio for Cit^{3-}:Y^{3+}). After vigorous stirring for 1 h, 2 mmol of Na_3VO_4 was introduced into the solution. After additional agitation for 1 h, the as-obtained mixing solution was transferred into a Teflon bottle held in a stainless steel autoclave, sealed, and maintained at 180 °C for 24 h. As the autoclave cooled to room temperature naturally, the precipitates were separated by centrifugation, washed with ethanol and deionized water in sequence, and then dried in air

---

(11) (a) Li, Y. Y.; Liu, J. P.; Huang, X. T.; Li, G. Y. *Cryst. Growth Des.* **2007**, *7*, 1350. (b) Zhang, Z.; Sun, H.; Shao, X.; Li, D.; Yu, H.; Han, M. *Adv. Mater.* **2005**, *17*, 42. (c) Gu, Z. J.; Zhai, T. Y.; Gao, B. F.; Sheng, X. H.; Wang, Y. B.; Fu, H. B.; Ma, Y.; Yao, J. N. *J. Phys. Chem. B* **2006**, *110*, 23829. (d) Wang, W. N.; Iskandar, F.; Okuyama, K.; Shinomiya, Y. *Adv. Mater.* **2008**, *20*, 3422.

(12) Lao, J. Y.; Wen, J. G.; Ren, Z. F. *Nano Lett.* **2002**, *2*, 1287.

(13) Shen, G. Z.; Bando, Y.; Golberg, D. *Appl. Phys. Lett.* **2006**, *88*, 123107.

(14) Xu, Z. H.; Li, C. X.; Li, G. G.; Chai, R. T.; Peng, C.; Yang, D. M.; Lin, J. *J. Phys. Chem. C* **2010**, *114*, 2573.

(15) (a) Carlos, L. D.; Ferreira, R. A. S.; Pereira, R. N.; Assuncao, M.; Bermudez, V. D. *J. Phys. Chem. B* **2004**, *108*, 14924. (b) Carlos, L. D.; Bermudez, V. D.; Ferreira, R. A. S.; Marques, L.; Assuncao, M. *Chem. Mater.* **1999**, *11*, 581. (c) Wang, J. W.; Tanner, P. A. *J. Am. Chem. Soc.* **2010**, *132*, 947. (d) Tanner, P. A.; Fu, L. S.; Cheng, B. M. *J. Phys. Chem. C* **2009**, *113*, 10773. (e) Zhang, F.; Wan, Y.; Shi, Y. F.; Tu, B.; Zhao, D. Y. *Chem. Mater.* **2008**, *20*, 3778. (f) Zhang, F.; Wan, Y.; Yu, T.; Zhang, F. Q.; Shi, Y. F.; Xie, S. H.; Li, Y. G.; Xu, L.; Tu, B.; Zhao, D. Y. *Angew. Chem., Int. Ed.* **2007**, *46*, 7976.

(16) Zimer, H.; Albers, K.; Wittrock, U. *Opt. Lett.* **2004**, *29*, 2761.

(17) (a) Fang, Z. M.; Hong, Q.; Zhou, Z. H.; Dai, S. J.; Weng, W. Z.; Wan, H. L. *Catal. Lett.* **1999**, *61*, 39. (b) Martínez-Huerta, M. V.; Coronado, J. M.; Fernández-García, M.; Iglesias-Juez, A.; Deo, G.; Fierro, J. L. G.; Banres, M. A. *J. Catal.* **2004**, *225*, 240.

(18) Terada, Y.; Shimamura, K.; Kochurikhin, V. V.; Barashov, L. V.; Ivanov, M. A.; Fukuda, T. *J. Cryst. Growth* **1996**, *167*, 369.

(19) (a) Huignard, A.; Gacoin, T.; Boilot, J. P. *Chem. Mater.* **2000**, *12*, 1090. (b) Li, G. C.; Chao, K.; Peng, H. R.; Chen, K. Z. *J. Phys. Chem. C* **2008**, *112*, 6228. (c) Maunders, E. A.; Deshazer, L. G. *J. Opt. Soc. Am.* **1971**, *61*, 684. (d) O'Connor, J. R. *Appl. Phys. Lett.* **1966**, *9*, 407. (e) Fields, R. A.; Birnbaum, M.; Fincher, C. L. *Appl. Phys. Lett.* **1987**, *51*, 1885. (f) Levine, A. K.; Palilla, F. C. *Appl. Phys. Lett.* **1964**, *5*, 118. (g) Levine, A. K.; Palilla, F. C. *Electrochem. Technol.* **1966**, *4*, 16.

(20) (a) Haase, M.; Riwotzki, K.; Meyssamy, H.; Kornowski, A. *J. Alloys Compd.* **2000**, *303*, 191. (b) Yan, C. H.; Sun, L. D.; Liao, C. S. *Appl. Phys. Lett.* **2003**, *82*, 3511. (c) Sohn, K. -S.; Lee, J. M.; Shin, N. *Adv. Mater.* **2003**, *15*, 2081. (d) Sohn, K.-S.; Zeon, I. W.; Chang, H.; Lee, S. K.; Park, H. D. *Chem. Mater.* **2002**, *14*, 2140.

(21) (a) Schwarz, H. *Z. Anorg. Allg. Chem.* **1963**, *323*, 44. (b) Wanmaker, W. L.; Bril, A.; Vrugt, J. W.; Broos, J. *Philips Res. Rep.* **1966**, *21*, 270. (c) Brecher, C.; Samelson, H.; Lempicki, A.; Riley, R.; Peters, T. *Phys. Rev.* **1967**, *155*, 178. (d) Venikouas, G. E.; Powell, R. C. *J. Lumin.* **1978**, *16*, 29. (e) Riwotzki, K.; Haase, M. *J. Phys. Chem. B* **2001**, *105*, 12709.

(22) (a) Huignard, A.; Buissette, V.; Laurent, G.; Gacoin, T.; Boilot, J. P. *Chem. Mater.* **2002**, *14*, 2264. (b) Wu, H.; Xu, H. F.; Su, Q.; Chen, T. H.; Wu, M. M. *J. Mater. Chem.* **2003**, *13*, 1223.

(23) Yu, M.; Lin, J.; Wang, Z.; Fu, J.; Wang, S.; Zhang, H. J.; Han, Y. C. *Chem. Mater.* **2002**, *14*, 2224.

(24) Ekambaram, S.; Patil, K. C. *J. Alloys Compd.* **1995**, *217*, 104.

(25) Sun, L. D.; Zhang, Y. X.; Zhang, J.; Yan, C. H.; Liao, C. S.; Lu, Y. Q. *Solid State Commun.* **2002**, *124*, 35.

(26) Li, Y. H.; Hong, G. Y. *J. Solid State Chem.* **2005**, *178*, 645.

(27) Lim, B.; Jiang, M. J.; Tao, J.; Camargo, P. H. C.; Zhu, Y. M.; Xia, Y. N. *Adv. Funct. Mater.* **2008**, *18*, 1.

Table 1. Summary of the Experimental Conditions and the Corresponding Morphologies and Dimensions of the Samples[a]

samples	vanadium source	organic additive	molar ratio	morphology	diameter	thickness or length
P1	Na_3VO_4	Cit^{3-}	2:1	microdoughnut	1 μm	500 nm
P2	Na_3VO_4	Cit^{3-}	0	nanoparticle	15 nm	
P3	Na_3VO_4	Cit^{3-}	1:1	nanoparticle	20 nm	
P4	Na_3VO_4	Cit^{3-}	3:1	micropancake	650 nm	130 nm
P5	Na_3VO_4	Cit^{3-}	4:1	pillar structure	450 nm	a few micrometers
P6	NH_4VO_3	Cit^{3-}	2:1	microflower	280 nm	
P7	Na_3VO_4	AO	2:1	square nanoplate	500−800 nm	50 nm
P8	Na_3VO_4	PVP	2:1	nanoparticle	20 nm	
P9	Na_3VO_4	Na_2tar	2:1	microdisk	200−500 nm	50 nm
P10	Na_3VO_4	EDTA	2:1	rectangular microrod	350 nm	a few micrometers

[a] All samples were hydrothermally treated at 180 °C for 24 h.

at 80 °C for 12 h. The as-prepared product was denoted as sample **P1**. In addition, samples **P2**−**P5** were prepared with different molar ratios of Cit^{3-}:Y^{3+} and other conditions are the same as those for synthesizing sample **P1**. Sample **P6** was prepared by a similar procedure except for different vanadium sources. The experimental conditions are summarized in Table 1. It should be stated that all samples were hydrothermally treated at 180 °C for 24 h. Additionally, some other organic additives, such as ammonium oxalate (AO), polyvinylpyrrolidone (PVP), sodium tartrate (Na_2tar), and ethylenediamine tetraacetic acid disodium salt (EDTA) were also selected to investigate the dependence of the morphological properties of the samples (**P7**−**P10**) on these factors. A similar process was employed to prepare 5 mol % Ln^{3+} (Ln^{3+} = Eu^{3+}, Dy^{3+}, Sm^{3+}, and Er^{3+}) doped YVO_4 samples by using a proper amount of Eu_2O_3, Dy_2O_3, Sm_2O_3, and Er_2O_3 together with Y_2O_3 as the starting materials as described above.

2.2. Characterizations. Powder X-ray diffraction (XRD) measurements were performed on a Rigaku-Dmax 2500 diffractometer with Cu Kα radiation (λ = 0.15405 nm). The morphology and structure of the samples were inspected using a field emission scanning electron microscopy (FE-SEM, XL 30, Philips) equipped with energy-dispersive X-ray (EDX) spectrometer and a transmission electron microscope. Low- to high-resolution transmission electron microscopy (TEM) was performed using FEI Tecnai G2 S-Twin with a field emission gun operating at 200 kV. Images were acquired digitally on a Gatan multiople CCD camera. The PL excitation and emission spectra were recorded with a Hitachi F-4500 spectrophotometer equipped with a 150 W xenon lamp as the excitation source. Photoluminescence quantum yield (QY) was measured by a C9920−02 absolute PL quantum yield measurement system from Hamamatsu (Japan). The cathodoluminescent (CL) measurements were carried out in an ultrahigh-vacuum chamber ($< 10^{-8}$ Torr), where the samples were excited by an electron beam at a voltage range of 1−5 kV with different filament currents, and the spectra were recorded on an F-4500 spectrophotometer. All measurements were performed at room temperature.

3. Results and Discussion

3.1. Structures. The composition and phase purity of the products were first examined by XRD. XRD patterns of the samples by using Na_3VO_4 as vanadium source with hydrothermal treatment at 180 °C for 24 h under different molar ratios of Cit^{3-}:Y^{3+} are shown in Figure 1A-E. The diffraction peaks of the samples **P1**−**P5** can be indexed as a pure tetragonal phase of YVO_4 with the cell parameters a = 7.119 Å and c = 6.289 Å (JCPDS No. 17-0341). Substitution of NH_4VO_3 for Na_3VO_4 as vanadium source, gives the XRD pattern of the as-prepared product (sample **P6**) shown in Figure 1F. As can be seen from the XRD patterns, all the peaks of samples can also be indexed as a pure tetragonal phase of YVO_4. Moreover, high crystallinity can be obtained at a relatively low hydrothermal treatment temperature (180 °C). This is important for phosphors because higher crystallinity generally means less defects and stronger luminescence.

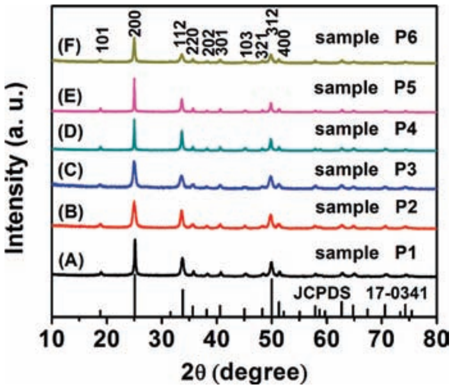

Figure 1. XRD patterns of the as-prepared samples (**P1**−**P6**). The standard data of YVO_4 (JCPDS 17-0341) was used as reference.

3.2. Morphologies. The morphologies and dimensions of the products are summarized in Table 1. From Table 1 it is found that vanadium sources, different organic additives, and the molar ratio of Cit^{3-}:Y^{3+} are predominantly influencing factors in the determination of the shapes and sizes of the final products, which will be discussed in the following paragraphs.

A. Na_3VO_4 as Vanadium Source. The SEM and TEM images provide direct information about the sizes and typical shapes of the as-synthesized YVO_4 samples grown under different experimental conditions. Figure 2 illustrates the representative SEM and TEM images of the sample **P1** prepared by using Na_3VO_4 as the vanadium source and Cit^{3-} as the organic additive at the Cit^{3-}/Y^{3+} molar ratio of 2:1. The sample **P1** is composed of uniform and doughnut-like YVO_4 hierarchical structures, as shown in Figure 2A. There is a concave dip in each center of the YVO_4 microdoughnut. The average size of the as-prepared product is about 1 μm in diameter and 500 nm in thickness. The higher magnification SEM images shown in Figure 2B,C reveal that each doughnut is composed of many layers of nanoscale sheet-like structures. These nanosheets are arranged at progressively increasing angles to the radial axis and are highly directed to form arrays in a regular fashion. The side view of an individual doughnut structure supports the conclusion that such microarchitecture is composed of densely packed nanosheets with an average thickness of about 10 nm.

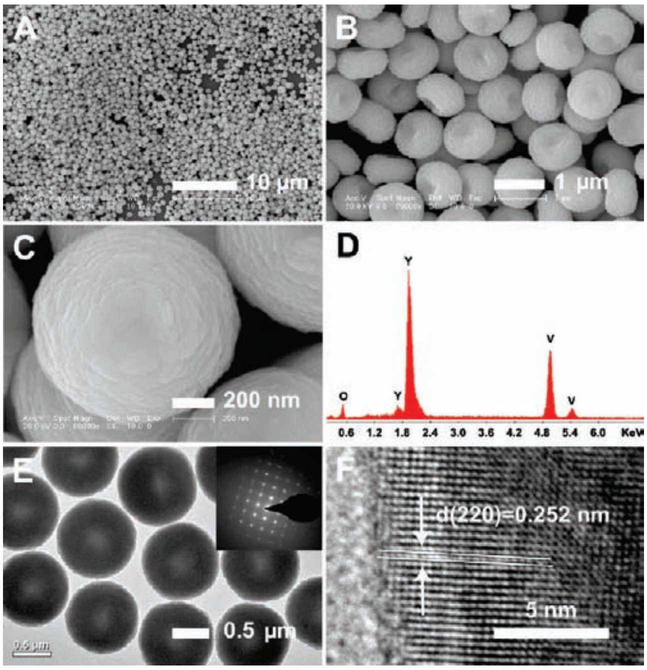

Figure 2. (A, B, C) SEM, (D) EDX spectrum, (E) TEM, and (F) HRTEM images for the as-prepared YVO_4 microdoughnuts (**P1**) using Na_3VO_4 as vanadium source. The inset of (E) is the corresponding SAED pattern taken from a single microstructure.

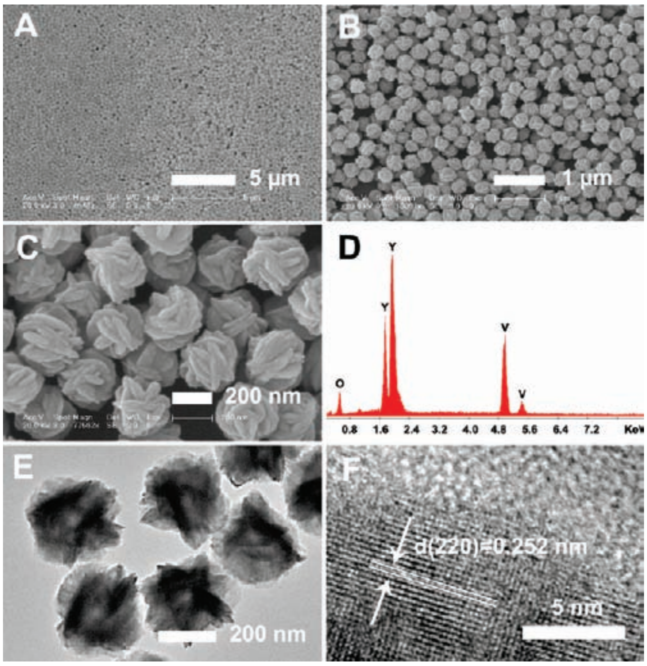

Figure 3. (A, B, C) SEM, (D) EDX spectrum, (E) TEM and (F) HRTEM images for the as-prepared YVO_4 microflowers (**P6**) using NH_4VO_3 as vanadium source.

Figure 2D shows the EDX pattern for the YVO_4 microdoughnut, which reveals the presence of Y, V, and O. More structural details of the sample were further investigated by TEM, high-resolution transmission electron microscopy (HRTEM), and selected area electron diffraction (SAED) pattern. The TEM image (Figure 2E) of YVO_4 doughnuts clearly shows that the sample has a spherical shape. The different contrast between the central and fringe part of an individual architecture also implies the concave dip exists in the center of products. The SAED pattern (inset in Figure 2E) taken from the discretional nanoplate indicates that the assembled nanoplate has a well-defined single-crystalline structure. As disclosed by the corresponding HRTEM (Figure 2F), the interplanar distance between the adjacent lattice fringes is determined to be 0.252 nm that corresponds to the (220) plane of the YVO_4 phase.

B. NH_4VO_3 as Vanadium Source. When NH_4VO_3 replaces Na_3VO_4 as vanadium source under the otherwise same reaction conditions, the morphologies of the products become quite different, as shown in Figure 3. Nearly monodisperse flower-like microstructures (**P6**) with average diameter of around 280 nm are shown in Figure 3A,B. Further close investigation under higher magnification also reveals that a single flower-like microstructure is composed of many petal-like nanoflakes with smooth surfaces and uniform thickness of about 40 nm (Figure 3C). The microarchitectures are loose and highly porous, and most of the nanoflakes are linked together by both edge-to-edge and edge-to-surface conjunctions; the nanoflakes extend outward from the center of the microstructure, and a few are attached to each other. The chemical composition of the YVO_4 microflowers was further investigated with EDX, which indicates that the microflowers are made of Y, V, and O (Figure 3D). Further information about the YVO_4 product was obtained from TEM and HRTEM images. Figure 3E shows a typical TEM image of a flowerlike YVO_4 microstructure, confirming that the hierarchical 3D structure with diameter of around 280 nm is constructed by numerous nanoflakes. Figure 3F is the HRTEM image for YVO_4, which reveals that the lattice plane of the microflowers afforded is highly crystallized, and the interplanar spacing of 0.252 nm that is coincident with (220) plane of YVO_4 phase.

C. Role of Organic Additive Cit^{3-}. In the synthesis of inorganic nano/microcrystals many organic additives have been employed for the modifications of certain crystallographic surfaces.[28] In our current system, we found that the Cit^{3-} plays a key role in the formation of YVO_4 architectures, independent of the vanadium source used. The Cit^{3-} is a strong chelating agent with three carboxylate groups for metal ions. It reacts with Y^{3+} to form stable Y^{3+}-Cit^{3-} complexes through stronger coordination interaction. According to LaMer's model, the formation of such complexes could control the concentration of free Y^{3+} ions in solution, and thus help to control the nucleation and growth of the crystals in the view of dynamic process.[29] The relatively slow generation rate of nanoparticles is favorable for the subsequent growth of 3D hierarchical nanostructures. To investigate the influence of

---

(28) (a) Li, F.; Ding, Y.; Gao, P.; Xin, X. Q.; Wang, Z. L. *Angew. Chem., Int. Ed.* **2004**, *43*, 5238. (b) Kuo, C.; Kuo, T. J.; Huang, M. H. *J. Phys. Chem. B* **2005**, *109*, 20115. (c) Shi, W. D.; Huo, L. H.; Wang, H. S.; Zhang, H. J.; Yang, J. H.; Wei, P. H. *Nanotechnology* **2006**, *17*, 2918. (d) Jana, N. R.; Gearheart, L. A.; Obare, S. O.; Johnson, C. J.; Edler, K. J.; Mann, S.; Murphy, C. J. *J. Mater. Chem.* **2002**, *12*, 2909. (e) Li, C. X.; Yang, J.; Yang, P. P.; Zhang, X. M.; Lian, H. Z.; Lin, J. *Cryst. Growth Des.* **2008**, *8*, 923. (f) Zhuang, J. L.; Wang, J.; Yang, X. F.; Williams, I. D.; Zhang, W.; Zhang, Q. Y.; Feng, Z. M.; Yang, Z. M.; Liang, C. L.; Wu, M. M.; Su, Q. *Chem. Mater.* **2009**, *21*, 160. (g) Zhuang, J. L.; Liang, L. F.; Sung, H. H. Y.; Yang, X. F.; Wu, M. M.; Williams, I. D.; Feng, S. H.; Su, Q. *Inorg. Chem.* **2007**, *46*, 5404.

(29) Li, Z. Q.; Zhang, Y. *Angew. Chem., Int. Ed.* **2006**, *45*, 7732.

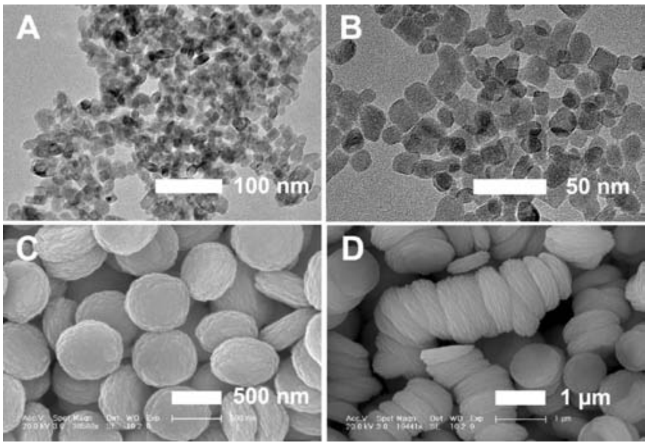

Figure 4. SEM images of the as-prepared YVO_4 samples (**P2**−**P5**) with different molar ratios of Cit^{3-}:Y^{3+} using Na_3VO_4 as vanadium source. (A) 0 (without Cit^{3-}), (B) 1:1, (C) 2:1, (D) 4:1.

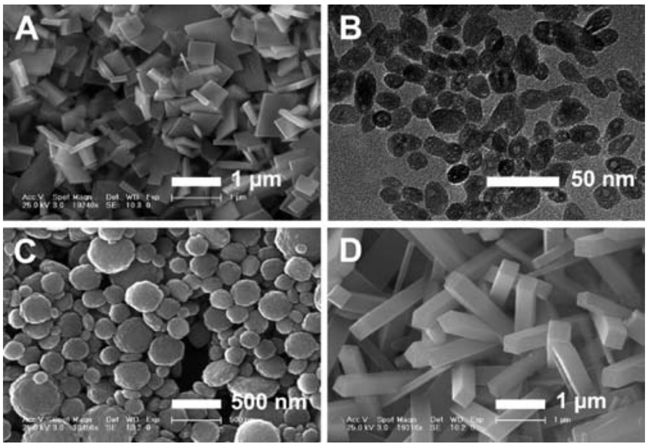

Figure 5. SEM images of the as-prepared YVO_4 samples (**P7**−**P10**) formed in the presence of (A) AO, (B) PVP, (C) Na_2tar, and (D) EDTA.

Cit^{3-} on the shape evolution in our current synthesis, we also conducted a series of parallel experiments to substantiate the role of Cit^{3-} in the shape control of products by altering its contents. Table 1 lists the changes in morphology and particle size for YVO_4 samples (**P2**−**P5**) prepared with the different molar ratios of Cit^{3-}:Y^{3+} (0, 1:1, 3:1, and 4:1) while the other conditions keep unchanged. Note that the crystalline phases of the as-prepared products remain unchanged (Figure 1B−E). However, the corresponding morphologies have drastic change, as shown in Figure 4. Without the use of Cit^{3-} (sample **P2**), many much smaller irregular shaped nanoparticles can be observed (Figure 4A), and the average size of the nanoparticles is about 15 nm. Quasi-sphere nanoparticles were obtained if the molar ratio of Cit^{3-}:Y^{3+} was 1:1 (sample **P3**; Figure 4B). The average size of these nanoparticles is about 20 nm. Further increasing the amount of Cit^{3-}, the Cit^{3-}:Y^{3+} molar ratio was increased to 3:1 (sample **P4**), the morphologies of the sample **P4** are pancake-like hierarchical structures (Figure 4C). The rough surface and evident boundaries of the obtained 2D pancake-like patterns indicate that an individual architecture is composed of many thin nanoplates with 30 nm in thickness, and these original nanoplates are self-assembled into an integrated structure along the longitudinal axis direction through face-to-face attachment. At the higher ratio of 4:1 (sample **P5**), it is interesting to find that the sample consists of pillar structures, assembled from micropancakes through face-to-face and layer-by-layer tight stacking style along the [001] direction, and with a length up to a few micrometers, as shown in Figure 4D. From the morphological evolutions discussed above, we can conclude that organic additive Cit^{3-} has an important influence on the morphologies of the final products in our current synthesis.

In a solution-phase synthesis, various organic additives are used to direct rationally the anisotropic growth of the crystals. When the vanadium source is fixed, four types of organic additives, ammonium oxalate (AO), polyvinylpyrrolidone (PVP), sodium tartrate (Na_2tar), and ethylenediamine tetraacetic acid disodium salt (EDTA), are used to perform the contrasting experiments with an aim to investigate their effects on the morphologies of the products through different coordination modes and specific molecular complementarity with yttrium orthovanadate. When other experimental conditions are identical as **P1** and these four organic additives are used, the shapes of the products (**P7**−**P10**) are quite different from the former. The as-formed product (**P7**) with AO as the organic additive is mainly composed of square nanoplates (Figure 5A). In the presence of PVP, the product (**P8**) is nanoparticles (Figure 5B). When Na_2tar or EDTA is employed as organic additive, the as-obtained products (**P9** or **P10**) take microdisks or cuboid microrods, as illustrated in Figure 5C, D, respectively. Generally, EDTA and Cit^{3-} have similar properties because they are regarded as excellent chelating agents that slow down the nucleation rate and prevent further aggregation of the particles.[30] However, they have a remarkably different impact on the morphologies of the final products, which is related to the differences of the chelating constant with Y^{3+} and the adsorption ability of the different crystal facets of YVO_4 particles. For example, the chelating constant is larger for EDTA ($\log \beta = 18-19$) than for Cit^{3-} ($\log \beta = 8-9$),[31] leading to the different nucleation rates of YVO_4. The smaller the chelating constant, the faster the nucleation rate. On the other hand, the coordination modes between EDTA and Cit^{3-} with Y^{3+} are clearly different,[32] so the selective adsorption binding on the specific crystal facets of YVO_4 particles is different, resulting in the different morphologies and sizes of the products. These results indicate that the organic additives have a remarkably different impact on the morphologies of the final products, which is related to the differences of the chelating constant with Y^{3+} and the adsorption ability of the different crystal facets of final products.

D. Effect of the Reaction Time. The morphologies of the samples were carefully investigated by taking out the autoclave from the oven to quench the reaction at different time intervals, which is used to understand the shape evolution of the crystals. It is found that the size of the obtained monodisperse YVO_4 architecture can be easily tuned by the reaction time. Figure 6 shows the SEM

---

[30] (a) Luo, F.; Jia, C. J.; Song, W.; You, L. P.; Yan, C. H. *Cryst. Growth Des.* **2005**, *5*, 137. (b) Tao, F.; Wang, Z. J.; Yao, L. Z.; Cai, W. L.; Li, X. G. *Cryst. Growth Des.* **2007**, *7*, 854.

[31] Moeller, T.; Martin, D. F.; Thompson, L. C.; Ferrús, R.; Feistel, G. R.; Randall, W. J. *Chem. Rev.* **1965**, *65*, 1.

[32] Sun, Y. J.; Chen, Y.; Tian, L. J.; Yu, Y.; Kong, X. G.; Zhao, J. W.; Zhang, H. *Nanotechnology* **2007**, *18*, 275609.

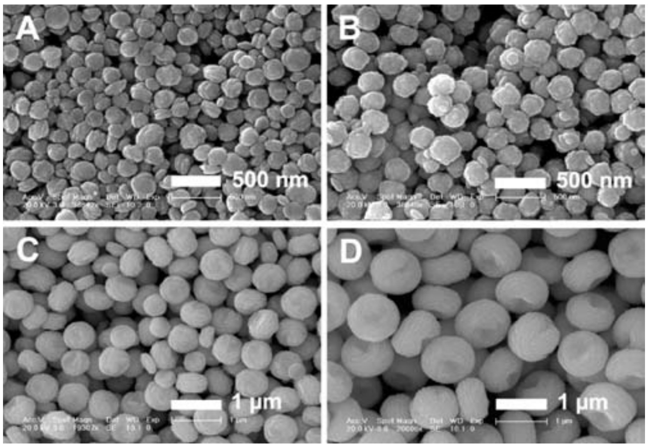

Figure 6. SEM images for YVO_4 samples under similar conditions for synthesizing **P1** as a function of reaction time of (A) 2 h, (B) 6 h, (C) 12 h, and (D) 24 h.

images of the corresponding intermediates. At t = 2 h, nearly monodispersed architectures with a mean diameter of about 200 nm are obtained (Figure 6A). If the reaction time was prolonged to 6, 12, or 24 h, a uniform and monodisperse architecture with a pancake shape was obtained. But, careful observations of the magnified images (Figure 6B−D) indicate that the architecture aggregates increase gradually in size with the reaction proceeding, and the corresponding diameters are 270 nm, 600 nm, 1 μm, respectively, and the thickness increases from 50 to 500 nm. Therefore, in this process, more nanoflakes are needed to generate and assemble into the microarchitecture to make it grow, which means that this is not a on-off nucleation−growth process but a continual nucleation−growth process.[33]

3.3. Formation Mechanism for the YVO_4 Microarchitecture. On the basis of the above analysis, we can confirm that the growth of YVO_4 microarchitecture is directly related to the function of the organic molecules (Cit^{3-}). Laudise et al.[34] claimed that the growth of crystals is related to the relative growth rate of different crystal facets, and the difference in the growth rates of various crystal facets results in a different shape of the crystallite. In a solution-phase synthesis, organic additives acting as surfactants or capping agents can change the order of free energies of different facets through their interaction with metal surface. This alteration may significantly affect the relative growth rates of different facets. Enlightened by our experimental results and the previous reports,[14,28e,35] a plausible process for the self-assembly of the YVO_4 microarchitecture is shown in Scheme 1. At first, Cit^{3-} ions react with Y^{3+} to form Y^{3+}-Cit^{3-} complexes, greatly decreasing the free Y^{3+} ion concentration in solution. Then under hydrothermal conditions (high temperature and pressure), the chelating of the Y^{3+}-Cit^{3-} complex is attacked by $VO_4{}^{3-}$ and an anion-exchange reaction between $VO_4{}^{3-}$ and Cit^{3-} would take place, and then Y^{3+} would be released gradually. This competition reaction can slow down the nucleation and subsequent crystal growth of YVO_4 nuclei. During the subsequent crystal growth stage, Cit^{3-} anions possibly bind selectively to the active (001) facet of the growing precursor nanoparticles. Thus the crystal growth along [001] orientation is inhibited to some degree, and it grows preferentially along [100] and [010] directions. It is worth noting that because of the usage of different parameters such as vanadium source and the molar ratio of organic additive trisodium citrate (Cit^{3-}):Y^{3+}, the growth environment of the crystals are different, so the selective adsorption of Cit^{3-} on the different facets of growing YVO_4 crystallites, resulting in that the relative growth rates of YVO_4 along the [001] versus [100] directions are different. As a consequence, the products achieved under the different experimental conditions take a wealth of shapes of structures such as nanoparticles, microdoughnuts, micropancakes, pillar structures, and microflowers. The whole formation mechanism of different products is presented in Scheme 1.

From the above results, it is apparent that the cooperative action of the inherent structure features of different YVO_4 crystal phases and organic additive Cit^{3-} leads to the variation of the shapes of the products in both the absence and the presence of Cit^{3-}. To sum up, Cit^{3-} species may have a double function on the growth of the precursor. First, as a strong ligand, it can form a stable complex with Y^{3+} ions, which slows down the nucleation and subsequent crystal growth of the precursor microarchitecture. Second, Cit^{3-} acts as a structure-directing reagent binding to the surface of crystals, which directly affects the growth of different crystal facets by adjusting the growth rate of different facets, resulting in the formation of the microurchin structure. In fact, the mechanism for the formation of the multiform morphologies is very complicated because of several factors, including crystal-face attraction, electrostatic and dipolar fields associated with the aggregate, van der Waals forces, hydrophobic interactions, and hydrogen bonds, and may have various effects on the self-assembly.[36]

3.4. Photoluminescence Properties of Ln^{3+} (Ln = Eu, Dy, Sm, and Er)-Doped YVO_4. It is noted that all Ln^{3+}-doped YVO_4 samples could be prepared in a similar procedure as for synthesizing **P1**. All the doping ratios of Ln^{3+} are molar in our experiments. The luminescent properties of the YVO_4:Ln^{3+} samples were explored by monitoring their multicolor emission in the visible region on single-wavelength light excitation. Figure 7 shows the excitation and emission spectra of the as-prepared YVO_4: Ln^{3+} samples. The excitation spectrum (Figure 7A, left) of YVO_4: 5 mol % Eu^{3+} consists of a strong absorption band with a maximum at 291 nm and several weak lines. The strong absorption band is due to the charge transfer from the oxygen ligands to the central vanadium ions inside the $VO_4{}^{3-}$ groups. The weak lines are attributed to the f → f transitions within the $4f^6$ configuration of the Eu^{3+} ions. The absorption intensity of the general f → f transitions of the Eu^{3+} ions in the longer wavelength region is very weak in comparison with that of the $VO_4{}^{3-}$

---

[33] Chen, Z.; Bu, W.; Zhang, N.; Shi, J. *J. Phys. Chem. C* **2008**, *112*, 4378.

[34] (a) Laudise, R. A.; Ballman, A. A. *J. Phys. Chem.* **1960**, *64*, 688. (b) Laudise, R. A.; Kolb, E. D.; Caporaso, A. J. *J. Am. Ceram. Soc.* **1964**, *47*, 9.

[35] (a) Qian, L.; Zhu, J.; Chen, Z.; Gui, Y. C.; Gong, Q.; Yuan, Y. P.; Zai, J. T.; Qian, X. F. *Chem.—Eur. J.* **2009**, *5*, 1233. (b) Li, C. X.; Quan, Z. W.; Yang, J.; Yang, P. P.; Lin, J. *Inorg. Chem.* **2007**, *46*, 6329. (c) Li, C. X.; Quan, Z. W.; Yang, P. P.; Yang, J.; Lian, H. Z.; Lin, J. *J. Mater. Chem.* **2008**, *18*, 1353.

[36] (a) Politi, Y.; Arad, T.; Klein, E.; Weiner, S.; Addadi, L. *Science* **2004**, *306*, 1161. (b) Colfen, H.; Antonietti, M. *Angew. Chem., Int. Ed.* **2005**, *44*, 5576. (c) Colfen, H.; Mann, S. *Angew. Chem., Int. Ed.* **2003**, *42*, 2350.

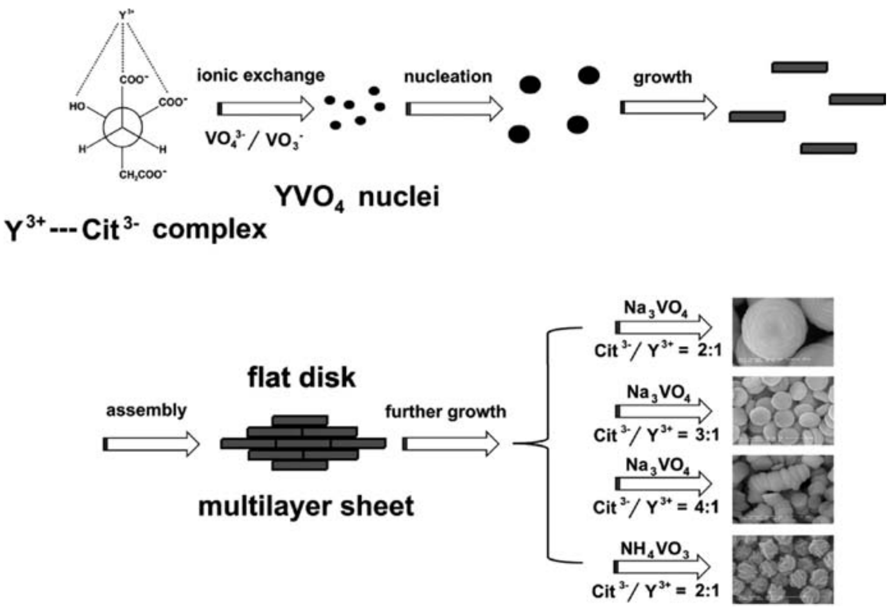

Scheme 1. Schematic Illustration for the Possible Formation Mechanism of YVO_4 with Various Morphologies under Different Experimental Conditions

groups, indicating that the excitation of the Eu^{3+} ions is mainly through the VO_4^{3-} groups. The emission spectrum (Figure 7A, right) exhibits five groups of emission lines between 539 and 700 nm, which are ascribed to the $^5D_1 \rightarrow {}^7F_1$ and $^5D_0 \rightarrow {}^7F_J$ (J = 1, 2, 3, 4) transitions of the Eu^{3+} ions, respectively. No emission from the VO_4^{3-} groups was observed, revealing that the energy transfer from the VO_4^{3-} groups to Eu^{3+} ions is very efficient.[37] The emission spectrum is dominated by the red $^5D_0 \rightarrow {}^7F_2$ (619 nm) transition of the Eu^{3+} ions, because of a forced electric-dipole transition of the Eu^{3+} ions in YVO_4. The whole excitation and emission process of YVO_4:Eu^{3+} under UV radiation include three major steps. The first is absorption of UV radiation by VO_4^{3-} groups, then the excited energy is subsequently transferred to Eu^{3+} ions after a thermally activated energy migration through the vanadate sublattice, and the final one is the de-excitation process of excited Eu^{3+} ions, producing strong red emissions. The excitation and emission process of VO_4^{3-} and the energy transfer process from VO_4^{3-} to Eu^{3+}, as well as the emission process of Eu^{3+}, are schematically shown in Figure 8A. The strong red emission of the sample upon excitation at 254 nm with a UV lamp can be seen clearly (inset of Figure 7A). The photograph confirms the strong red emission of the YVO_4: 5 mol % Eu^{3+} sample. The chromaticity coordinates (CIE) of YVO_4: 5 mol % Eu^{3+} sample are x = 0.675 and y = 0.301, located in the red region (Figure 8, point a), which agrees well with the luminescence photograph (inset in Figure 7A). The PL absolute QY value for the as-obtained YVO_4:Eu^{3+} sample is 70% under the excitation of 285 nm.

The room-temperature excitation and emission spectra of the other rare earth ions Dy^{3+}-, Sm^{3+}-, and Er^{3+}-doped YVO_4 samples are given in Figure 7B, C, and D, respectively. The excitation spectra for YVO_4: 5 mol % Sm^{3+}, YVO_4: 5 mol % Dy^{3+}, and YVO_4: 5 mol % Er^{3+} samples are very similar to YVO_4: 5 mol % Eu^{3+} sample (Figure 7A, right); that is, monitored with 576 nm emission of Dy^{3+} ($^4F_{9/2} \rightarrow {}^6H_{13/2}$), 604 nm emission of Sm^{3+} ($^4G_{5/2} \rightarrow {}^6H_{7/2}$), and 554 nm emission of Er^{3+} ($^4S_{3/2} \rightarrow {}^4I_{15/2}$), respectively, a strong and broad band due to the VO_4^{3-} group has been observed. The characteristic emissions of these luminescent lanthanide ions can also be observed after excitation in the charge-transfer band of the vanadate groups. For Ln = Dy, as indicated in Figure 7B, the emissions at 485 and 576 nm are associated with the typical transitions from the $^4F_{9/2}$ level to the $^6H_{15/2}$ and $^6H_{13/2}$, respectively. For Ln = Sm (Figure 7C), a red-orange light was observed, which consists of the typical emissions at 565, 604, and 649 nm that originate from the transitions from the $^4G_{5/2}$ level to the $^6H_{5/2}$, $^6H_{7/2}$, and $^6H_{9/2}$ levels, respectively. Figure 7D exhibits the emission spectrum of YVO_4: 5 mol % Er^{3+} sample which originate from the transitions $^2H_{11/2} \rightarrow {}^4I_{15/2}$ and $^4S_{3/2} \rightarrow {}^4I_{15/2}$ at 527 and 554 nm, respectively. These indicate that the same situation holds for Dy^{3+}-, Sm^{3+}-, and Er^{3+}-doped YVO_4 samples, that is, an efficient energy transfer also occurs from VO_4^{3-} to Dy^{3+}, Sm^{3+}, and Er^{3+}. From the above results and analysis, the emission color can be tuned by doping with different lanthanide activators. It can be confirmed by the CIE (Commission International de I'Eclairage 1931 chromaticity) coordinates for the emission spectra of the YVO_4:Ln^{3+} (Ln = Dy, Sm, and Er) samples (Figure 8). The YVO_4:Dy^{3+} sample emits green-yellow light and its chromaticity coordinates are x = 0.312 and y = 0.471. The YVO_4:Sm^{3+} and YVO_4:Er^{3+} samples can emit orange-red and green emissions, and the chromaticity coordinates are x = 0.615, y = 0.343 and x = 0.241, y = 0.716, respectively. Under the excitation of 285 nm the PL QY values for the as-obtained YVO_4:Ln^{3+} (Ln = Dy, Sm, and Er) samples are 62%, 50%, and 56%, respectively.

In addition, we also investigated the spectral and luminescent properties of the products with various

---

(37) Jia, G. H.; Tanner, P. A.; Cheng, B. M. *Chem. Phys. Lett.* **2009**, *474*, 97.

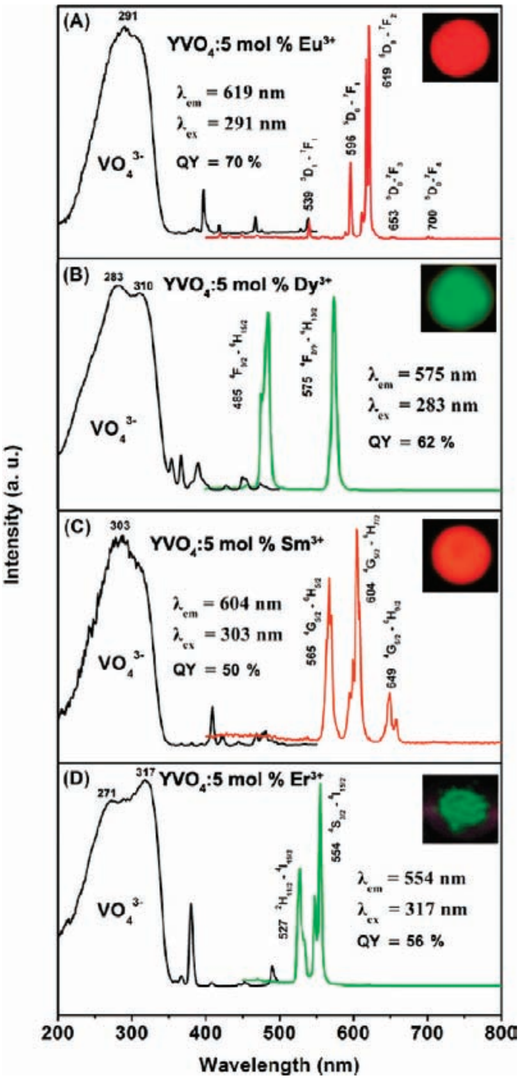

Figure 7. Excitation and emission spectra as well as quantum yield (QY) for YVO_4:5 mol % Eu^{3+} (A), YVO_4:5 mol % Dy^{3+} (B), YVO_4:5 mol % Sm^{3+} (C), and YVO_4:5 mol % Er^{3+} (D). The insets are the corresponding luminescence photographs of the samples upon excitation at 254 nm with an UV lamp.

morphologies. Figure 9 show the excitation and emission spectra as well as QY values of YVO_4:5 mol % Dy^{3+} samples with different shapes (**P7**−**P10**). It can be seen clearly that, in all four samples, the excitation and emission spectra are similar in shape, and the bands differ only in their intensities. This is because the excitation and emission of Dy^{3+} arise from f-f transitions which are strongly shielded by the outside 5s and 5p electrons. As a result, the excitation and emission spectra (peak positions) are not strongly dependent on the morphology of the YVO_4 host lattices. However, the PL emission intensities of YVO_4:5 mol % Dy^{3+} with four different morphologies/sizes are different under identical measurement conditions. Namely, the rectangular microrods (sample **P10**, black line) have the highest relative emission intensity, while the nanoparticles (sample **P8**, blue line) show the lowest intensity. It is well-known that the surface area of materials increases along with a decrease in size. The large surface area introduces a large number of defects into the phosphor crystal. Defects have serious drawbacks in PL intensity for phosphors as they provide non-radiative recombination routes for electrons and holes. To be as efficient as possible for the phosphors, the number of electron/hole recombinations via optically active centers must be

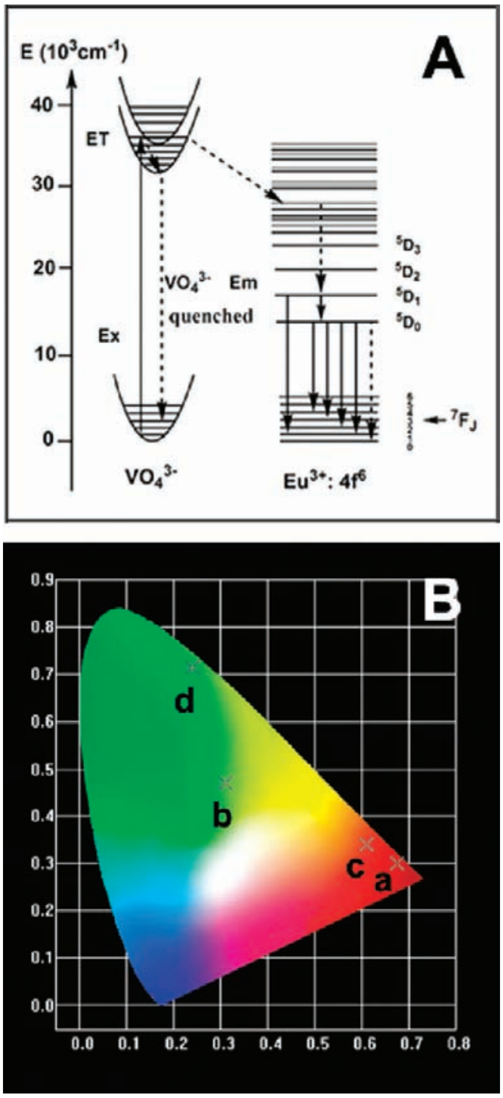

Figure 8. Scheme for VO_4^{3-}−Eu^{3+} energy transfer and Eu^{3+} emission process(A), and CIE chromaticity diagram of Eu^{3+} (point a), Dy^{3+} (point b), Sm^{3+} (point c), and Er^{3+} (point d) doped YVO_4 (B).

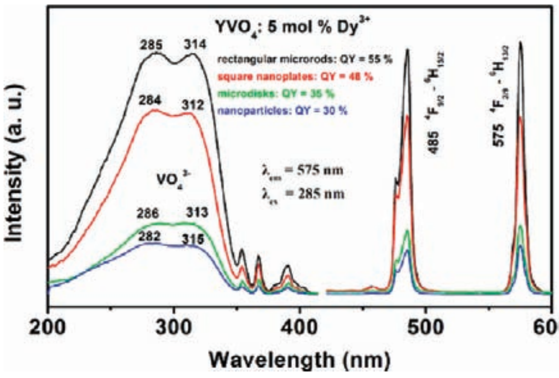

Figure 9. Excitation and emission spectra as well as quantum yield (QY) of YVO_4:5 mol % Dy^{3+} samples with different shapes.

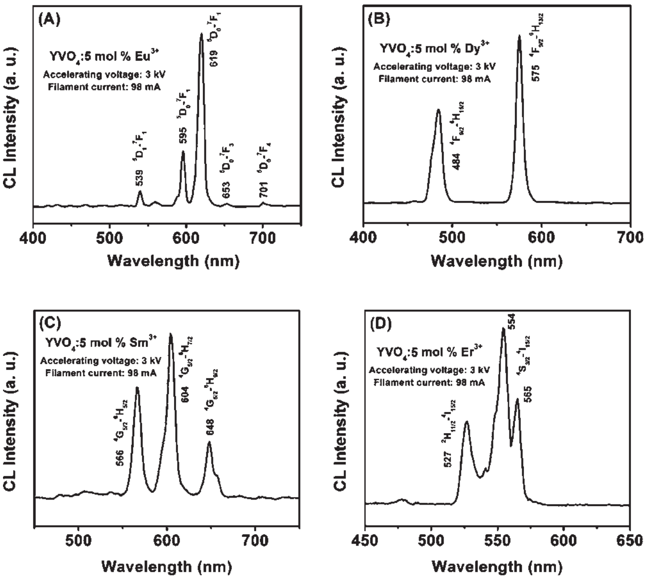

Figure 10. Typical cathodoluminescence spectra of (A) YVO$_4$: 5 mol % Eu^{3+}, (B) YVO$_4$: 5 mol % Dy^{3+}, (C) YVO$_4$: 5 mol % Sm^{3+}, and (D) YVO$_4$: 5 mol % Er^{3+} samples.

maximized. If the surface area is greatly reduced, which results from increased crystallite size, a phosphor with fewer defects would show great improvement in the PL intensity.[38] From the SEM results presented above (Figure 5), it can be observed that the surface area of the as-synthesized **P10** is smaller than those of **P7**, **P8**, and **P9** because **P10** is greater in size than **P7**, **P8**, and **P9**. Moreover, the measured absolute QY values of the **P7**−**P10** products are 48%, 30%, 35%, and 55%, respectively, in good agreement with the above emission intensity results.

3.5. Cathodoluminescence Properties of Ln^{3+} (Ln = Eu, Dy, Sm, and Er)-Doped YVO$_4$. Under low-voltage electron beam excitation, the as-prepared YVO$_4$:Ln^{3+} (Ln = Eu, Dy, Sm, and Er) samples also exhibit the same red, green-yellow, orange-red, and green emissions as the UV excitation, respectively. The representative CL spectra of the YVO$_4$:Ln^{3+} samples under the excitation of electron beam (accelerating voltage =3 kV; filament current = 98 mA) are shown in Figure 10, which have identical shapes as the PL emission spectra. However, the relative intensity of peaks in the photoluminescence and cathodoluminescence spectrum varies, which may be caused by the different excitation mechanism. The CL emission intensities for the YVO$_4$:Ln^{3+} samples have been investigated as a function of the filament current and the accelerating voltage respectively as shown in Figure 10. Under a 98 mA electron beam excitation, the CL intensity increased with the accelerating voltage from 3.5 to 5.5 kV (Figure 11A). Similarly, when the accelerating voltage is fixed at 5 kV, the CL intensity also increases with rising filament current from 92 to 104 mA (Figure 11B). The increase in CL brightness with increasing electron energy and filament current can be attributed to a deeper penetration of the electrons into the phosphors and the larger electron beam current density. The electron penetration depth can be estimated using the empirical formula L [Å] = 250(A/ρ)($E/Z^{1/2}$)^n, where n = 1.2/(1 − 0.29 log$_{10}$ Z), A is the atomic or molecular weight of the material, ρ is the bulk density, Z is the atomic number or the number of electrons per molecule in the case compounds, and E is the accelerating voltage (kV).[39] For cathodoluminescence, the Eu^{3+}, Dy^{3+}, Sm^{3+}, and Er^{3+} ions are excited by the plasma produced by the incident electrons. With the increase of accelerating voltage or filament current, more plasma will be produced, which resulted in more Eu^{3+}, Dy^{3+}, Sm^{3+}, and Er^{3+} ions being excited and thus the CL intensity increased. Because of the strong low voltage CL intensity and excellent dispersing properties of YVO$_4$:Ln^{3+} phosphors, they are potentially applicable in field emission display devices.

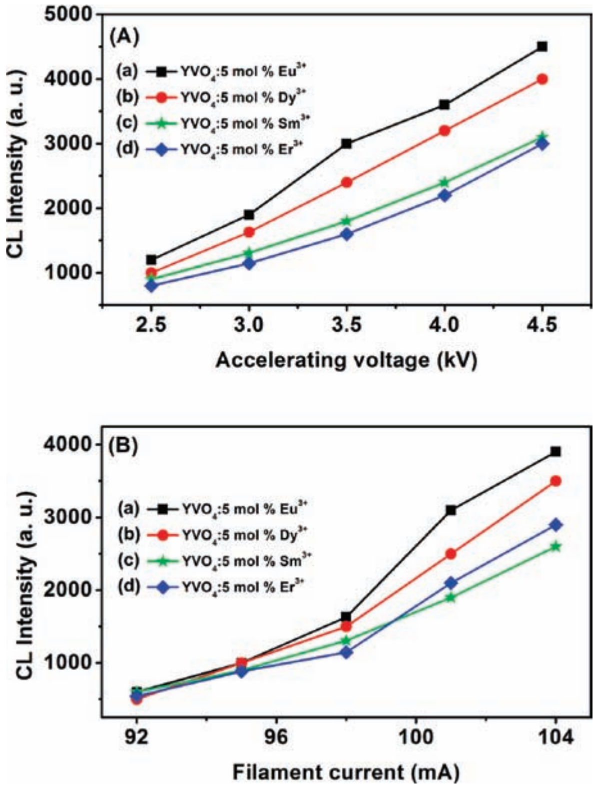

Figure 11. Cathodoluminescence intensity of YVO$_4$: Ln^{3+} (Ln = Eu, Dy, Sm, and Er) samples as a function of accelerating voltage (A) and filament current (B).

4. Conclusions

In summary, we have demonstrated a simple and mild hydrothermal method for the synthesis of YVO$_4$ nano/microcrystals with a broad range of regular and uniform shapes. A series of controlled experiments show that reaction time, vanadium sources, different organic additives, and molar ratio of organic additive trisodium citrate (Cit^{3-}): Y^{3+} have important influence on the shapes of the final products. Under ultraviolet or low-voltage electron beam excitation, the Ln^{3+} (Ln = Eu, Dy, Sm, and Er) ions doped YVO$_4$ samples show strong red, green-yellow, orange-red, and green, respectively. More importantly, under the excitation of 285 nm, the PL absolute quantum efficiencies for YVO$_4$:Ln^{3+} (Ln = Eu, Dy, Sm, and Er) samples obtained by

---

[38] (a) Yang, J.; Liu, X. M.; Li, C. X.; Quan, Z. W.; Kong, D. Y.; Lin, J. *J. Cryst. Growth.* **2007**, *303*, 480. (b) Yang, J.; Li, C. X.; Cheng, Z. Y.; Zhang, X. M.; Quan, Z. W.; Zhang, C. M.; Lin, J. *J. Phys. Chem. C* **2007**, *111*, 18148.

[39] Feldman, C. *Phys. Rev.* **1960**, *117*, 455.

this simple method are measured to be 70%, 62%, 50%, and 56%, respectively. These merits of multicolor emissions and higher quantum efficiency in the visible region endow this kind of material with potential application in the field of light display systems, lasers, and optoelectronic devices.

Acknowledgment. This project is financially supported by National Basic Research Program of China (2007CB935502, 2010CB327704), and the National Natural Science Foundation of China (NSFC 20901074, 50872131, 60977013, 20921002).